Optica Applicata, Vol. XLVII, No. 4, 2017
DOI: 10.5277/oa170403

Calculation of laser radar cross-section of a spatial object and its experimental verification

CAO YUN-HUA[1*], WANG ZHE[1], BAI LU[1], WU ZHENSEN[1, 2], LI HAI-YING[1], LI YAN-HUI[1]

[1]School of Physics and Optoelectronic Engineering, Xidian University, Xi'an, 710071, China

[2]Collaborative Innovation Center of Information Sensing and Understanding at Xidian University, Xi'an, 710071, China

[*]Corresponding author: yhcao@mail.xidian.edu.cn

Bidirectional reflectance distribution function of some artificial satellite used materials at the wavelength of 1.06 μm was measured in laboratory. Bidirectional reflectance distribution function (BRDF) models of these materials were established with the five-parameter BRDF model. Laser radar cross-section of a scaled satellite with various materials was calculated, and characteristics of laser radar cross-section of the satellite were discussed. Measurement system to measure laser radar cross-section of the satellite was established and the scaled satellite model was measured. By analyzing the measured data and calculated data, it can be clearly seen that the BRDF of the surface materials and the laser incidence angle are two of main influential factors of the scaled satellite's laser radar cross-section. These works can provide a reference for design of the lidar system.

Keywords: bidirectional reflectance distribution function (BRDF), laser radar cross-section (LRCS), spatial object.

1. Introduction

Laser scattering characteristics are important optical scattering properties of spatial objects, which play an important role in design and evaluation of laser detection systems [1]. Laser radar cross-section (LRCS) can be used to synthetically reflect an object's laser scattering characteristics which are produced by such factors as the surface material and coarseness, the geometrical structure, and the shape [2].

According to the relationship between the differential scattering coefficient and bidirectional reflectance distribution function (BRDF) [3], LRCS can be calculated with BRDF of materials on the spatial object. In previous studies, some researchers regarded satellite's materials as diffuse Lambert surfaces [4, 5]. This method simplified the calculation, but it did not conform to practical situation. Reference [6] evaluated

LRCS for some rotationally symmetrical objects such as cones, spheres, paraboloids and cylinders by use of different reflection characteristics. In fact, LRCS of these ideal targets are not suitable for some spatial objects which have complex geometry structure. In current correlative researches, LRCSs of a spatial object at different attitude angles and solar panel rotating angles have been calculated by a visualization method based on OpenGL which is one of developing environments for graphics applications and is used to accomplish the complicated calculation work including the geometry transformation, shading judgment and display of complex targets [7, 8]. Various BRDF measurement systems have been designed to measure BRDF of various materials [9–13]. We measured BRDF of some artificial satellite used materials such as solar panel, polyimide film, optical solar reflector (OSR) panel, and white paint at the wavelength of 1.06 μm in laboratory. The measured BRDF data were at special incidence and reflected angles. BRDF models of these materials were established based on the measured BRDF data and the five-parameter model [13]. With the obtained models, BRDF of these materials at arbitrary incidence and reflected angle can be obtained.

A scaled geometrical model of a simple satellite with a cubic body and solar panel wing was established. Then the model was divided into small facets dS, and each facet is assigned with a known BRDF model. As LRCS of each visible facet can be calculated with BRDF of the facet, LRCS of the satellite can be obtained by summating LRCS of each visible facet. LRCSs of the satellite at different incidence and reflected angles were calculated. Measurement system to measure LRCS of the satellite was established.

This text will expound the above-mentioned contents from four aspects. The basic theory of BRDF and LRCS and the relationship between them are described in Section 2. In Section 3, BRDF of satellite surface materials is calculated with models based on the five-parameter model and measured BRDF data. Section 4 presents the calculation of LRCS of the spatial object. In Section 5, LRCS measurement system and comparison between the calculation and the measured data are discussed.

2. Basic theory of BRDF and LRCS

BRDF was first proposed by NICODEMUS [14] to characterize a differential scattering surface. BRDF is defined as

$$f_r(\theta_i, \varphi_i, \theta_r, \varphi_r) = \frac{\mathrm{d}L_r(\theta_i, \varphi_i, \theta_r, \varphi_r)}{\mathrm{d}E_i(\theta_i, \varphi_i)} \tag{1}$$

where subscripts r and i denotes reflected and incident, respectively, θ – zenith angle, φ – azimuth angle; $\mathrm{d}L_r(\theta_i, \varphi_i, \theta_r, \varphi_r)$ is the differential radiance in the direction of (θ_r, φ_r), $\mathrm{d}E_i(\theta_i, \varphi_i)$ is the differential irradiance in the direction of (θ_i, φ_i), thus the BRDF is defined as the ratio of reflected radiance to the incident irradiance. The unit of BRDF is inverse steradian (sr^{-1}). The value range of BRDF is 0 to infinity.

When the concept of BRDF is applied to electromagnetic scattering from rough surfaces, the BRDF function can be rewritten as

$$f_{\mathrm{r}}(\theta_{\mathrm{i}}, \varphi_{\mathrm{i}}, \theta_{\mathrm{r}}, \varphi_{\mathrm{r}}) = \frac{\mathrm{d}P_{\mathrm{s}}}{P_i \cos(\theta_{\mathrm{r}})\mathrm{d}\Omega} \tag{2}$$

where P_{i} and $\mathrm{d}P_{\mathrm{s}}$ are the incident power and scattered power per unit area, respectively.

LRCS is used to quantitatively describe the lidar scattering characteristics. LRCS can be defined as

$$\sigma^0(\theta_{\mathrm{i}}, \varphi_{\mathrm{i}}, \theta_{\mathrm{r}}, \varphi_{\mathrm{r}}) = \lim_{R \to \infty}\left[4\pi R^2 \frac{\langle \mathbf{E}_{\mathrm{s}} \cdot \mathbf{E}_{\mathrm{s}}^* \rangle}{A_{\mathrm{i}}\left|\mathbf{E}_{\mathrm{i}}\right|^2}\right] \tag{3}$$

where A_{i} is the irradiated area, R is the distance between the target and the lidar, $\mathbf{E}_{\mathrm{s}}$ and $\mathbf{E}_{\mathrm{i}}$ are the scattering and incident fields, respectively, $\langle \cdot \rangle$ is the statistical average of the scattering field intensity. LRCS has the same unit as area, and in this paper, the unit of LRCS in calculation and measurement is m^2.

When the area of receiving aperture is A_{r}, the ratio of received scattered power ΔP_{s} and incident power P_{i} is

$$\frac{\Delta P_{\mathrm{s}}}{P_i} = \frac{A_{\mathrm{r}} \langle \mathbf{E}_{\mathrm{s}} \cdot \mathbf{E}_{\mathrm{s}}^* \rangle}{A_{\mathrm{i}} \cos(\theta_{\mathrm{i}}) \left|\mathbf{E}_{\mathrm{i}}\right|^2} \tag{4}$$

Associating Eq. (3) with Eq. (4), LRCS can be represented as

$$\sigma^0(\theta_{\mathrm{i}}, \varphi_{\mathrm{i}}, \theta_{\mathrm{r}}, \varphi_{\mathrm{r}}) = \lim_{R \to \infty}\left[\frac{4\pi R^2}{A_{\mathrm{r}}} \frac{\Delta P_{\mathrm{s}}}{P_i} \cos(\theta_{\mathrm{i}})\right] = 4\pi \cos(\theta_{\mathrm{i}}) \frac{\mathrm{d}P_{\mathrm{s}}}{P_i \mathrm{d}\Omega} \tag{5}$$

where $\mathrm{d}\Omega = \lim_{R \to \infty} (A_{\mathrm{r}}/R^2)$.

Substituting Eq. (2) into Eq. (5), the functional relation between BRDF and LRCS can be obtained:

$$\sigma^0(\theta_{\mathrm{i}}, \varphi_{\mathrm{i}}, \theta_{\mathrm{r}}, \varphi_{\mathrm{r}}) = 4\pi f_{\mathrm{r}} \cos(\theta_{\mathrm{i}}) \cos(\theta_{\mathrm{r}}) \tag{6}$$

3. Measurement and modeling of BRDF of satellite surface materials

BRDF of some satellite surface materials such as solar panel, polyimide film, OSR panel, and white paint at the wavelength of 1.06 μm was measured in laboratory. The measurement system used was the same as that in [13]. Calculating LRCS of spatial objects needs BRDF at arbitrary incidence and reflected angle, so BRDF model should be established. There are many BRDF models available [15–17], and a five-parameter BRDF model

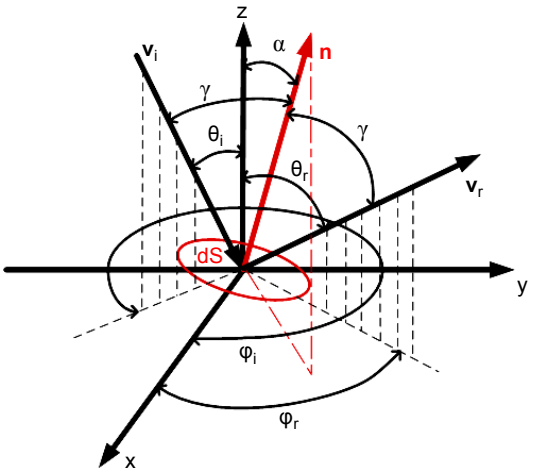

Fig. 1. The coordinate system of the five-parameter BRDF.

was used in this paper. The coordinate system of the five-parameter BRDF is shown in Fig. 1. We assume that the z axis coincides with the normal of the rough surface averaged plane, $\mathbf{v}_i$ is the incident vector, $\mathbf{v}_r$ is the scattered vector, θ is the zenith angle, φ is the azimuth angle, α is the angle between the normal direction **n** of the facet and the z axis, γ is the incident angle in the local coordinate of the facet.

The formula of the five-parameter BRDF model [13] is as follows:

$$f_r(\theta_i, \theta_r, \varphi_r) = k_b \frac{k_r^2 \cos(\alpha)}{1 + (k_r^2 - 1)\cos(\alpha)} \exp\{b[1 - \cos(\gamma)]^a\} \frac{G(\theta_i, \theta_r, \varphi_r)}{\cos(\theta_r)} + k_d \tag{7}$$

where the five parameters to be determined in the model are k_b, k_r, b, a and k_d. The parameter k_b is the specular reflection coefficient, k_d is the diffuse reflection coefficient which contains the contribution of multiple scattering, volume scattering and material optical properties. The function $k_r^2 \cos(\alpha)/[1 + (k_r^2 - 1)\cos(\alpha)]$ is the distribution of the normal of the facet. In spherical coordinates, the function is an ellipsoid of revolution, and the coefficient k_r is the ratio of the horizontal axis and vertical axis of the ellipsoid. $R_0(\gamma) = R(\gamma)/R(0)$ is the relative reflection coefficient of the facet. In the model, $R_0(\gamma)$ is approximately simulated by the exponential function $R_0(\gamma) = \exp\{b[1 - \cos(\gamma)^a]\}$, which can save a lot of calculation time consumed by the calculation of many trigonometric functions in the classical expression of Fresnel reflectance function. Parameters a and b are determined by the refractive index of medium, for example, when $R_0(\pi/2) = \exp(b) = R(\pi/2)/R(0) = (n + 1)^2/(n - 1)^2$, the initial value of b can be taken as $b = \ln[(n + 1)/(n - 1)]^2$, here n is the refractive index of medium. The shadowing function $G(\theta_i, \theta_r, \varphi_r)$ is determined by the probability of shadowing and masking, which occurred between the adjacent facets.

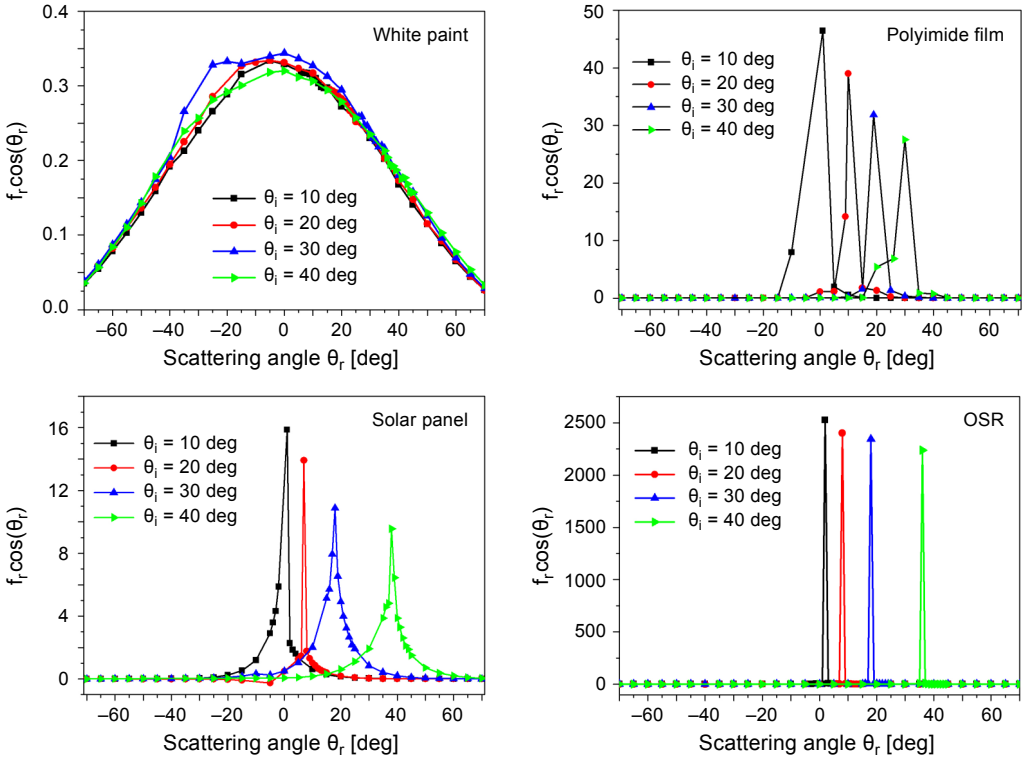

Fig. 2. Measured BRDF data of satellite surface materials at the incidence angle of 10, 20, 30 and 40 deg.

The measured data of satellite surface materials are shown in Fig. 2. In the figures, each line represents BRDF data of different incidence angle. The vertical axis in the figures represents BRDF multiplied by $\cos(\theta_r)$, and the horizontal axis represents the scattering angle θ_r. Optical characteristics of the satellite surface materials can be described by BRDF data shown in the figures. For example, BRDF data change slowly, which indicates that the white paint is approximately Lambert surface, and BRDF data change sharply which indicates that OSR panel is a mirror like material.

Genetic algorithm was used to optimize the parameters of the five-parameters BRDF model to fit the measured BRDF data. The least square error criterion function was used as the objective function of the genetic algorithm

T a b l e. Parameters in the five-parameter BRDF model of each satellite surface material.

Sample	k_b	k_r	b	a	k_d
OSR	2250.33	23.2027	–20.2674	0.121503	0.00065
Solar panel	12.5478	18.8405	–8.4518	0.216006	0.00451
Polyimide film	20.7111	0.78752	–20.0052	0.288088	0.09000
White paint	0.13500	0.27751	–14.2870	1.578048	0.29507

$$E(x) = \frac{\sum_{\theta_i} \sum_{\theta_r} \left[f_r(\theta_i, \theta_r, 0)\cos(\theta_r) - f_r^0(\theta_i, \theta_r, 0)\cos(\theta_r) \right]^2}{\sum_{\theta_i} \sum_{\theta_r} \left[f_r^0(\theta_i, \theta_r, 0)\cos(\theta_r) \right]^2} \tag{8}$$

where $f_r(\theta_i, \theta_r, 0)$ is the calculated BRDF value and $f_r^0(\theta_i, \theta_r, 0)$ is the measured BRDF data. The obtained parameters are shown in the Table. With the parameters, BRDF at arbitrary incidence and scattering angle can be calculated by Eq. (1).

4. Calculation of LRCS of spatial object

4.1. Theory on calculation of LRCS of spatial object

LRCS of spatial object can be obtained by integrating the differential scattering coefficient σ^0 over the visible surface of the object.

Procedure to calculate LRCS of a spatial object is shown in Fig. 3. Firstly, a geometrical model of the object will be created with the software 3ds Max, and then the model is divided into triangles. Secondly, by assigning materials to each triangle, the model composed of triangles with materials will be obtained. Thirdly, at given incidence and reflected angles, the visible triangles of the model can be obtained. Fourthly, with transformation of coordinates, incidence and reflected angles from normal of triangles can be obtained. Finally, with incidence and reflected angle from normal of each triangle and BRDF model of each triangle, LRCS of each visible triangle can be calculated as

$$\text{LRCS} = \sigma^0 S = 4\pi f_r \cos(\theta_i)\cos(\theta_r) S \tag{9}$$

where S is the area of the visible triangle. LRCS of the spatial object is summation of LRCS of all the visible triangles.

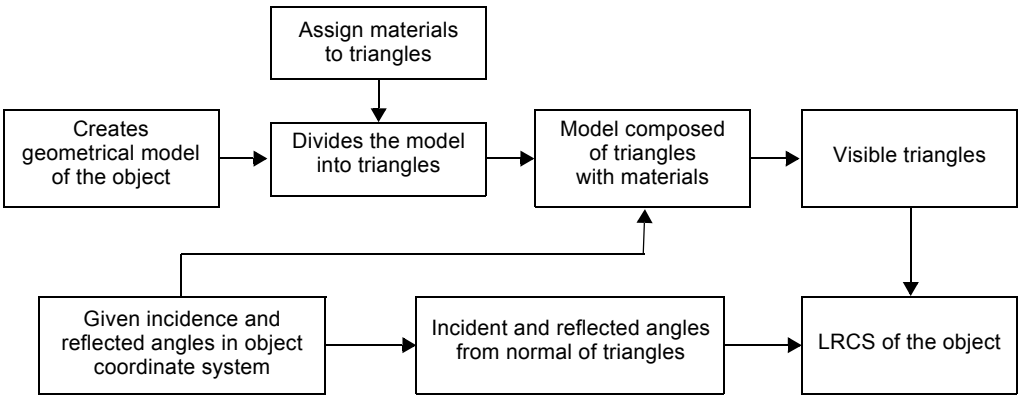

Fig. 3. Procedure to calculate LRCS of the spatial object.

4.2. Description of the spatial object

The spatial object researched in this paper is a scaled satellite shown in Fig. 4. The satellite is composed of a cubic main body and a wing. The size of the cube is (1.40 × 0.75 × 1.30) m, and the size of the wing is (2.55 × 1.11) m. And the object coordinate system is shown in the left top of Fig. 4.

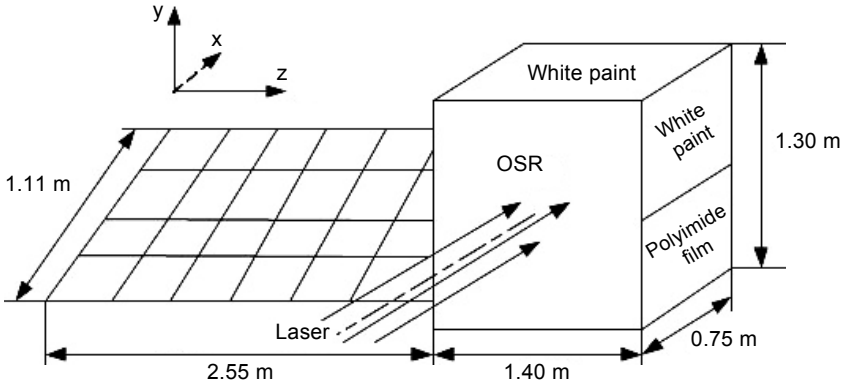

Fig. 4. Description of a scaled satellite.

The $-Y$ side of the wing is covered by solar panels, and $+Y$ side of the wing is the white paint. $+Y$ side of the cube is covered by white paint, $+X$ and $-X$ side are OSR, half of the $+Z$ side is white paint and the other half is polyimide film, $-Y$ and $-Z$ side is polyimide film. Pitch angle is defined as a rotation angle around the z-axis, azimuth angle is defined as a rotation angle around y-axis, and zenith angle is defined as a rotation angle around x-axis.

4.3. Analysis of calculation result

Part of the LRCS calculated data of the object is shown in Figs. 5 and 6. In Fig. 5, the azimuth angle of the object is –90 deg, and the zenith angle of the object is 180 deg. The incidence and receiving zenith angles are 5, 10, 15 and 20 deg, respectively. The incidence and receiving azimuth angle change from 0 to 360 deg. The initial position of incidence system is along the x-axis. In Fig. 6, the model remains stationary, while laser and receiver system move around y-axis. The incidence and receiving zenith angles are 1, 2, 3, 4, 5, 10, 15, 20, and 25 deg, respectively.

The results show that the main influence factors of LRCS of the satellite are BRDF of the material and incidence angle.

1) For a same target, the LRCS of diffuse materials is larger than LRCS of specular materials. As illustrated in Fig. 5, the maximum value of LRCS appears when the azimuth angle is 0, which is due to the fact that the laser illuminates at facets with white paint and it is a diffuse material. While when the azimuth angle is 90 deg, the facets

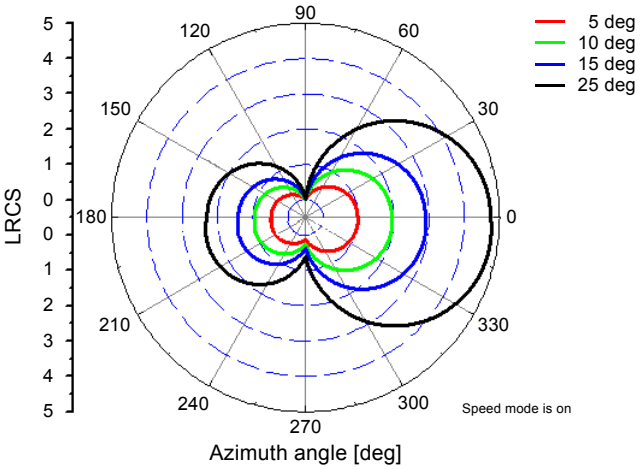

Fig. 5. Calculated data of LRCS of the object.

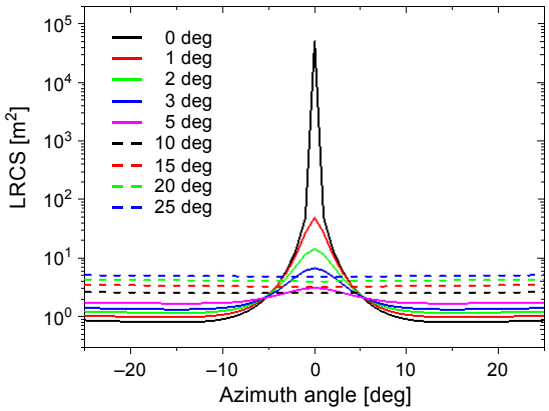

Fig. 6. Calculated data of LRCS when laser and receiver system move around *y*-axis.

material is a polyimide film which generates strong specular reflection, and the LRCS value is close to 0, consequently. When the azimuth angle is 270 deg, the laser would illuminate on +*Z* side, covered with mixed materials and half of which is white paint, so the LRCS value of +*Z* side is larger than LRCS value of –*Z* side covered with a polyimide film. When the azimuth angle is 180 deg, the laser incidents at –*Y* side of cube and the LRCS value is relatively large as the wing has a larger area.

2) LRCS increases with the zenith angle. The reason is that the projection of the illuminated surface increases when the zenith angle increases.

3) Effect of the incidence and receiving angle on LRCS for specular materials is much more obvious than it is for diffuse materials. The peak of LRCS of the satellite in Fig. 6 is very high at the specular reflection direction when the laser illuminates at facets with material of solar panel or OSR panel, and the value reduced quickly when

the incidence and reflected direction is away from the specular reflection direction. When the laser illuminated at facets with satellite coating material or white paint, LRCS varies slower.

5. Measurement of LRCS of the spatial object

5.1. Description of the measurement system

LRCS of the model is measured with a relative measurement method. Laser is collimated and extended before illuminating on the model to be measured, and through the receiver optical system, scattering light is collected to the detector. The final signal displayed on the display device is voltage. During measurement, laser and receiver system remain stationary. The receiving axis is parallel to the laser axis. Variation of incidence and scattering angles are obtained by adjusting the attitude of the model. Wavelength of the laser is 1.06 μm, and the distance between the laser device and the model to be measured is 100 m.

Voltages for the model and a standard diffuse reflection board at the same incidence and scattering angle are measured. LRCS of the model can be obtained by

$$\delta_1 = \frac{U_1}{U_0}\delta_0 \tag{10}$$

where δ_1 and δ_0 are LRCS of the model and the standard diffuse reflection board, respectively; U_1 and U_0 are the measured voltages for the model and the standard diffuse reflection board, respectively. And δ_0 can be obtained easily by

$$\delta_0 = Af_{r_0}\cos(\theta_i)\cos(\theta_r) \tag{11}$$

where A is the area of the standard board, f_{r_0} is BRDF of the standard board, θ_i and θ_r are the incidence and scattering angle. And BRDF of the standard diffuse reflection board is a constant, $f_{r_0} = \rho/\pi$ (and ρ is hemispherical directional reflectance of the standard board).

5.2. Comparison between the calculated and the measured data of LRCS

Laser is incident along the x-axis in the measurement. The object to be measured is the scaled satellite shown in Fig. 4. The comparison between the calculated and measured data of LRCS of the object is shown in Figs. 7 and 8. In the figures, discrete points represent the measured LRCS of the scaled satellite, and the solid line represents the calculated ones.

As OSR is especially smooth, and BRDF lines of OSR in Fig. 2 are very sharp, the peak of LRCS in Figs. 7 and 8 is very sharp. In Fig. 8, LRCS increases when the pitch angle varies from 10 to 45 deg, which is the contribution of white paint on $+Y$ side of the cube. As white paint is approximately Lambert surface, LRCS increases when the

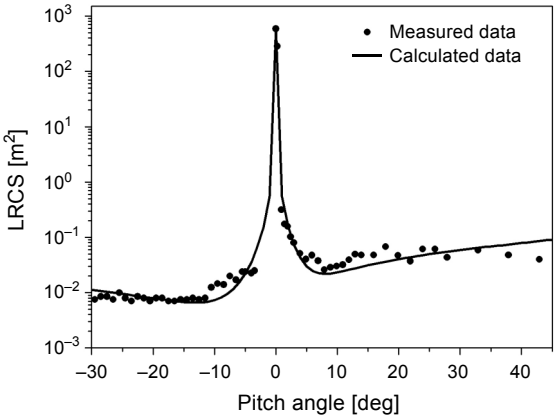

Fig. 7. Comparison of measured and calculated data when the object rotates around the *z*-axis.

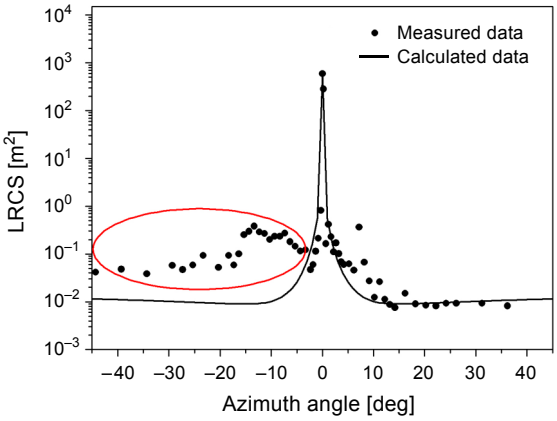

Fig. 8. Comparison of measured and calculated data when the object rotates around the *y*-axis.

area being illuminated increases. Because polyimide film is folded when it is covered on the cube, the measured LRCS data is larger than the calculated ones, when azimuth angle varies from –45 to –5 deg. At other angles, the measured data and calculated data show good consistency.

6. Conclusion

LRCS of a scaled satellite at the wavelength of 1.06 μm was calculated with BRDF of materials on the spatial object. Based on the calculated data, we obtained the conclusion that the BRDF of the material and laser incidence angle are the main influential factors of LRCS of the satellite. For the same target, the LRCS of diffuse materials is larger than LRCS of specular materials. The sensitivity of LRCS to the laser incidence angle is high for specular materials while it is very low for diffuse materials.

LRCS of the scaled satellite model was also measured to verify the calculation. The result shows that the measured data and calculated data are basically identical, so the calculation method is accurate and rapid. In the calculation, the effect of sunlight and surface material's fold was not taken into consideration, which caused some minor errors. In future work, more factors will be taken into account for reducing error and making the calculation more conform with actual situation. And more suitable BRDF models will be selected for popularization and application. The BRDF parameters of different materials will be measured to build a database. These works provide a more efficient condition for calculation of LRCS of different complex objects. It can be used to predict a target's laser scattering characteristics and design or evaluate lidar system.

Acknowledgments – This work was funded by the National Natural Science Foundation of China (Nos. 61475123 and 61571355).

References

[1] HUAYAN SUN, YI HAN, HUICHAO GUO, *Study of the laser scattering characteristic of space objects*, Proceedings of SPIE **7494**, 2009, article ID 74940J.

[2] SUN PENG-JU, GAO WEI, WANG YUE-FENG, *Calculation and application of laser radar cross section for targets*, Infrared and Laser Engineering **35**(5), 2006, pp. 597–598.

[3] TOMIYASU K., *Relationship between and measurement of differential scattering coefficient (σ^0) and bidirectional reflectance distribution function (BRDF)*, IEEE Transactions on Geoscience and Remote Sensing **26**(5), 1988, pp. 660–665.

[4] LUKESH G.W., CHANDLER S.M., BARNARD C.C., *Estimation of satellite laser optical cross section: a comparison of simulations and field results*, Proceedings of SPIE **4167**, 2001, pp. 53–63.

[5] LUKESH G.W., CHANDLER S.M., VOELZ D.G., *Analysis of satellite laser optical cross sections from the active imaging testbed*, Proceedings of SPIE **4538**, 2002, pp. 24–33.

[6] STEINVALL O., *Effects of target shape and reflection on laser radar cross sections*, Applied Optics **39**(24), 2000, pp. 4381–4391.

[7] HAN YI, SUN HUA-YAN, LI YING-CHUN, TANG LI-MING, *Simulation of space object laser radar cross section*, Infrared and Laser Engineering **39**(5), 2010, pp. 819–823.

[8] HAN YI, SUN HUAYAN, LI YINGCHUN, GUO HUICHAO, *Fast calculation method of complex space targets' optical cross section*, Applied Optics **52**(17), 2013, pp. 4013–4019.

[9] HONGSONG LI, SING-CHOONG FOO, TORRANCE K.E., WESTIN S.H., *Automated three-axis gonioreflectometer for computer graphics applications*, Optical Engineering **45**(4), 2006, article ID 043605.

[10] PAPETTI T.J., WALKER W.E., KEFFER C.E., JOHNSON B.E., *MRDF and BRDF measurements of low -scatter materials*, Proceedings of SPIE **6550**, 2007, article ID 65500H.

[11] OBEIN G., AUDENAERT J., GED G., LELOUP F.B., *Metrological issues related to BRDF measurements around the specular direction in the particular case of glossy surfaces*, Proceedings of SPIE **9398**, 2015, article ID 93980D.

[12] HEGEDUS R., LUCAT A., REDON J., PACANOWSKI R., *Isotropic BRDF measurements with quantified uncertainties*, [In] *Workshop on Material Appearance Modeling*, [Eds.] R. Klein, H. Rushmeier, The Eurographics Association, 2016.

[13] HANLU ZHANG, ZHENSEN WU, YUNHUA CAO, GENG ZHANG, *Measurement and statistical modeling of BRDF of various samples*, Optica Applicata **40**(1), 2010, pp. 197–208.

[14] NICODEMUS F.E., *Directional reflectance and emissivity of an opaque surface*, Applied Optics **4**(7), 1965, pp. 767–775.

[15] ELHAM KALANTARI, YUSUF ESHQI MOLAN, *Analytical BRDF model for rough surfaces*, Optik – International Journal for Light and Electron Optics **127**(3), 2016, pp. 1049–1055.
[16] RENHORN I.G.E., HALLBERG T., BOREMAN G.D., *Efficient polarimetric BRDF model*, Optics Express **23**(24), 2015, pp. 31253–31273.
[17] BUTLER S.D., NAUYOKS S.E., MARCINIAK M.A., *Comparison of microfacet BRDF model to modified Beckmann–Kirchhoff BRDF model for rough and smooth surfaces*, Optics Express **23**(22), 2015, pp. 29100–29112.

Received November 1, 2016
in revised form February 22, 2017